Synthesis and Characterisation of Zeolite-A and Zn Exchange Zeolite-A based on Natural Aluminosilicates and their Potential Applications

Article *in* Cogent Engineering · February 2018

DOI: 10.1080/23311916.2018.1440480

CITATION
1

READS
293

7 authors, including:

E. Nyankson
University of Ghana
27 PUBLICATIONS **193** CITATIONS
SEE PROFILE

Johnson Kwame Efavi
University of Ghana
42 PUBLICATIONS **322** CITATIONS
SEE PROFILE

Abu Yaya
University of Ghana
55 PUBLICATIONS **303** CITATIONS
SEE PROFILE

Gloria Manu
University of Ghana
2 PUBLICATIONS **2** CITATIONS
SEE PROFILE

cogent engineering

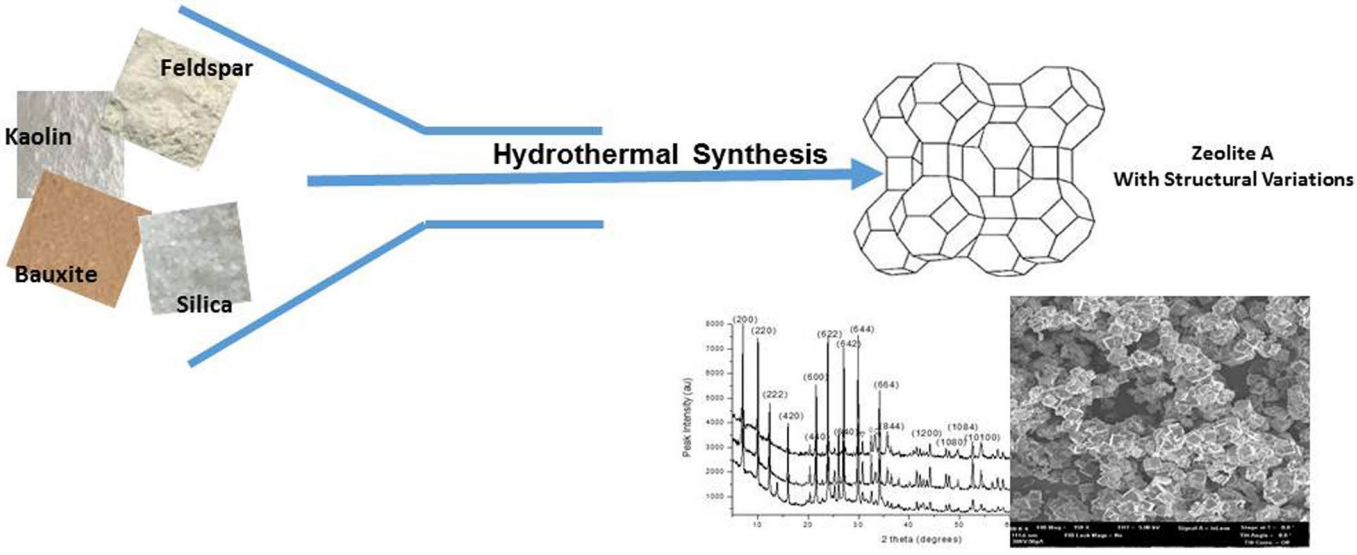

MATERIALS ENGINEERING | RESEARCH ARTICLE

Synthesis and characterisation of zeolite-A and Zn-exchanged zeolite-A based on natural aluminosilicates and their potential applications

Emmanuel Nyankson, Johnson Kwame Efavi, Abu Yaya, Gloria Manu, Kingsford Asare, Joseph Daafuor and Richard Yeboah Abrokwah

Cogent Engineering (2018), 5: 1440480

cogent oa

Nyankson et al., *Cogent Engineering* (2018), 5: 1440480
https://doi.org/10.1080/23311916.2018.1440480

cogent engineering

MATERIALS ENGINEERING | RESEARCH ARTICLE

Synthesis and characterisation of zeolite-A and Zn-exchanged zeolite-A based on natural aluminosilicates and their potential applications

Emmanuel Nyankson[1], Johnson Kwame Efavi[1]*, Abu Yaya[1], Gloria Manu[1], Kingsford Asare[1], Joseph Daafuor[1] and Richard Yeboah Abrokwah[2]

Received: 14 September 2017
Accepted: 11 February 2018
First Published: 15 February 2018

*Corresponding author: Johnson Kwame Efavi, School of Engineering Sciences, Department of Materials Science & Engineering, University of Ghana, P.O. BOX LG 74, Accra, Ghana
E-mail: jkefavi@ug.edu.gh

Reviewing editor:
Mohamed M. Rashad, Central Metallurgical Research and Development Institute, Egypt

Additional information is available at the end of the article

Abstract: Zeolites have been hydrothermally synthesized using alumina and silica based deposits (kaolin, bauxite, silica and feldspar) sampled from three regions in Ghana and the chemical compositions of the zeolites varied by batch formulations. The as-synthesized zeolites were characterized using X-ray Diffraction, Fourier Transform Infra-Red and Porosimetry techniques. The morphology and elemental compositions were examined using Scanning Electron Microscopy and energy dispersive X-ray spectroscopy (EDX). The results indicate that zeolite A was formed with a cubic structure and structural variations depending on the batch formulations. By increasing the silica content (Si/Al ratio) through batch formulations, the crystallite sizes of zeolites increased forming Zeolite A with LTA structure and Zeolite A (K-exchanged dehydrated). Samples with higher alumina content produced Zeolite A (Hydrated), Zeolite-Na and Zeolite A (Na, Dehydrated) with lower crystallite sizes. The zeolite synthesized was then used in the synthesis of zinc exchanged Zeolite A (Zn-zeolite A). EDX analysis confirmed a complete exchange of Na in the Zeolite framework with Zn and the feasibility as an adsorbent for methylene blue tested. The synthesized Zn-exchanged Zeolite A showed strong adsorption for methylene

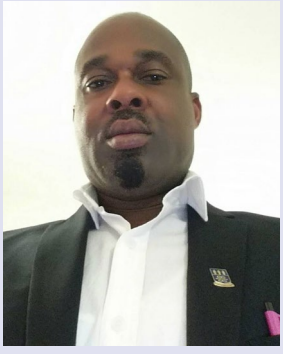

Johnson Kwame Efavi

ABOUT THE AUTHORS

Johnson Kwame Efavi is a senior lecturer at the Department of Materials Science & Engineering, University of Ghana, Ghana. He obtained his PhD in Electronic Materials with a speciality in functional materials- preparation, synthesis/processing and application at RWTH Aachen University, Germany in 2007. Some of his current research works involve synthesis and functionalisation of nano porous materials from local raw materials. Emmanuel Nyankson is a lecturer at the Department of Materials Science and Engineering, University of Ghana and he has immense expertise in the nano-catalyst synthesis for environmental remediation. Abu Yaya's research interest is in computational materials modelling of nano-systems and composite materials. Richard Yeboah Abrokwah is a researcher with North Carolina A &T, USA and has wealth of experience in porous materials development for industrial application. Kingsford Asare and Joseph Daafuor are materials science graduate students at School of Engineering Sciences, CBAS, University of Ghana, Ghana.

PUBLIC INTEREST STATEMENT

This work explores the feasibility of synthesising and functionalising zeolites a nano porous material medium from local raw materials. The Si/Al ratio in zeolite frameworks affects its efficiency when used as a catalyst diverse application. One of the approaches that can be used in tuning the functional capabilities of zeolites is to use batch formulation of natural aluminosilicates with different contents of Si and Al impregnated with transition based metals. Zeolites and its composites have been studied extensively for decades and their catalytic capabilities have been established. Using batch formulations we explore a simple method for the development of zeolites for the first time from batch formulations of kaolin, bauxite, feldspar, and silica deposits and then test their feasibility as an absorbent medium for dye removal in aqueous solutions. Zn exchanged zeolites shows positive catalytic effect in removing dyes from aqueous medium.

blue dye. The adsorption kinetics of the MB onto Zn-exchanged Zeolite A was observed to follow pseudo-second-order model. Freundlich model better described the interaction among adsorbate molecules onto the Zn-exchanged Zeolite A adsorbent, suggesting a multilayer distribution of adsorbate molecules with some level of interaction between adsorbed molecules. The regeneration capacity of the adsorbent was low and calculated to be about 48% at pH of 12.

Subjects: Materials Science; Nanoscience & Nanotechnology; Mining, Mineral & Petroleum Engineering; Chemical Engineering

Keywords: crystallinity; FTIR; kaolin; SEM; porous; XRD; Zn-exchanged Zeolite A; adsorbent; kinetics

1. Introduction

Zeolites and the its structural variations belong to a large class of porous materials referred to as ceramic molecular sieves and are hydrothermally very stable materials (Vu, Armbruster, & Martin, 2016; Zaarour, Dong, Naydenova, Retoux, & Mintova, 2014). The inherent sieve-like properties are exploited widely in catalysis, ion-exchange, water purification, membrane separation processes, solar cell application, drug delivery and antimicrobial applications (Atienzar, Valencia, Corma, & García, 2007; Barton et al., 1999; Daramola, Aransiola, & Ojumu, 2012; Rahmani, Azizi, & Asemi, 2016).

Conventional zeolites are microporous, hydrated aluminosilicates made up of alkali or alkaline earth metals and with a well-defined pore structure (Cejka, Corma, & Zones, 2010). Their frameworks are built by $[SiO_4]^{4-}$ and $[AlO_4]^{5-}$ tetrahedral (Gougazeh & Buhl, 2014; Ugal, Hassan, & Ali, 2010). The tetrahedra are linked together to form cages connected by pore openings of defined size and they are of the general formula $Mx/n[(AlO_2)x\ (SiO_2)y]\cdot zH_2O$ (Petrov & Michalev, 2012). M defines the compensating cation (usually from groups I or II) with valence n. Their properties are strongly influenced by the Si/Al ratio of the zeolite framework and the amount of cations control the surface properties as well as their adsorbent, catalytic and ion-exchange properties (Corma, Fornes, Navarro, & Perezpariente, 1994; Corma, Rey, Valencia, Jordá, & Rius, 2003; Hassani, Najafpour, Mohammadi, & Rabiee, 2014; Talesh, Fatemi, Hashemi, & Ghasemi, 2010).

Several research works have been done on zeolites and in most cases it has been observed that Si/Al ratio influences greatly the type of zeolites produced as well as the final crystal structure (Sharma, Han, & Cho, 2015; Shirazi, Jamshidi, & Ghasemi, 2008). Pérez-Pariente, Dïaz, Mohino, and Sastre (2003), studied the selective synthesis of fatty monoglycerides with zeolites and found that, catalytic properties have more effects on monoglyceride yield as compared with reaction parameters (Carrero, Vicente, Rodríguez, Linares, & del Peso, 2011; Pérez-Pariente et al., 2003). Also, Sasidharan and Kumar (2004) examining the effect of the pore size on the transesterification process of biodiesel production found out that large pore-zeolites like zeolite Y, Mordenite, showed higher activity (biodiesel yield) than the medium-pore zeolites because the large pores of zeolites favoured reaction by rendering the active sites more accessible to the bulky triglyceride molecules (Sasidharan & Kumar, 2004). Kwakye-Awuah, Von-Kiti, Nkrumah, and Williams (2013) synthesized zeolite from kaolin and bauxite sources and studied about the effect of the crystallization time on the crystallinity of zeolites and found out that crystallinity of zeolites increases with crystallization time (Kwakye-Awuah et al., 2013). Several research works have also shown that the nature of their porous framework has a strong effect on the efficiency as an absorbent or host materials in drug delivery as well as catalytic applications (Koohsaryan & Anbia, 2016).

The advantages of zeolites over other molecular sieves is as a result of their shape selective structures provided by the size and shape of the inner pore structures resulting in three forms of selectivity: reactant selectivity which allows introduction of small reactants into porous framework, transition state selectivity in which intermediates of appropriate sizes are formed and the last is

product selectivity which enables specific product to be formed (Seidel & Bickford, 2013). These inherent characteristics allow selection of molecules with regards to their size and shape thereby controlling their passage in the porous network and reactants with active sites. The use of conventional zeolites in a number of applications have been successful however, their use have molecular size limitations because of the intrinsic microporous nature of the pore system. This allows only active sites close to the pore entrances or their external surfaces which is calculated to be less than 10% of the total number of active sites to be available for active participation and accessibility of relatively bigger molecules in reactions. These observations have heightened interest in the search of innovative structural modification of the conventional zeolite framework to generate secondary pores in the porous system (Tang et al., 2006) and a mechanism for enhancing their redox catalytic path ways. Some notable strategies that have been adopted include introduction of secondary pores with sizes larger than 2 nm (meso, macro) and a process that reduces the crystal size to nanometer scale to give what is term as hierarchical and nanosized zeolites respectively (Tang et al., 2006) as well as functionalization of the structure using transition metals or metal oxides.

On the other hand the presence of $[AlO_4]^-$ in the zeolite structure introduces a negative charge which is compensated by protons leading to the formation of strong Brønsted acid sites (Marakatti, Halgeri, & Shanbhag, 2014). The presence and number of acid sites Lewis or Brønsted can be manipulated or exploited in numerous applications (Opanasenko et al., 2013). Dyes used in the textile industry cause significant environmental and health problems. It has been reported that, these dyes are toxic to human and aquatic animals (Alver & Metin, 2012; Benkli, Can, Turan, & Çelik, 2005; Wang & Ariyanto, 2007). To reduce their effect on the environment, different biological, chemical and physical methods such as coagulation, electrochemical techniques, ozonation and fungal decolorization has been used (Hameed, Ahmad, & Aziz, 2007; Wang & Zhu, 2006). However, none of these methods has been successful in completely removing dyes from waste water and this has increased the interest in the search of alternative simple methods. Variations of zeolite systems has been reported to be effective in removing dyes, heavy metal ions, pesticides and other organic pollutants from water. Dyes can be classified as anionic, cationic and nonionic. Adsorption of anionic dyes by zeolite has been reported to be low due to the fact that both zeolite and anionic dyes have similar surface charge characteristic (Eftekhari, Habibi-Yangjeh, & Sohrabnezhad, 2010; Wang & Peng, 2010; Wang & Zhu, 2006). The adsorption of anionic dyes by zeolite has been enhanced by modifying the surface of zeolite with hexamethylenediamine (HMDA) (Alver & Metin, 2012), hexadecyltrimethylammonium bromide (HTAB) (Benkli et al., 2005) and cetyltrimethylammonium bromide (CTAB) (Wang & Peng, 2010). The charge characteristics of zeolite can be modified to enhance its adsorption towards cationic dyes by introducing functional groups or using metal ion exchange in the zeolites framework to increase the number of acidic sites (Esquivel, Cruz-Cabeza, Jiménez-Sanchidrián, & Romero-Salguero, 2013; Goursot, Coq, & Fajula, 2003; Qi & Yang, 2005). The degree of ion exchange is reported to be dependent on the size and charge of the metal ion (Marakatti et al., 2014). Ion exchange of zeolite in zinc acetate solution can be used to achieve this purpose. Modification of zeolite with Zn(II) to form Zn-zeolite is expected to modify the surface charge characteristics of zeolite due to generation of new Lewis acid sites and variation of redox properties of the zeolites (Esquivel et al., 2013). This is expected to influence the selective adsorption of cationic dyes.

Different aluminosilicate based natural ores have different silicon and aluminium composition and we hypothesize that batch formulations of different natural deposits of such kind will result in different structural form of zeolites. In this work, we explore a simple method for the development of zeolites for the first time from batch formulations of kaolin, bauxite, feldspar, and silica deposits and then test the feasibility of the zeolites as an absorbent medium for dye removal in aqueous solutions. Different aluminosilicate based natural deposits have been sampled for this investigation. The kaolin was sampled from Kibi in the Eastern region of Ghana, the bauxite from Ghana Bauxite Co. Awaso, in the Western region of Ghana, while the feldspar and silica were sampled from Akyem Akroso and Akwatia respectively, all in the Eastern region of Ghana. The chemical composition of the batch formulations (Si and Al content) of the synthesized zeolites have been varied by batch formulations of the kaolin, bauxite, feldspar and silica deposits. The synthesized zeolites were

Table 1. Mineralogy and particle size of raw materials

Mineralogy	Particle size (μm)
Kaolin	≤75
Feldspar	≤75
Silica	≤75
Bauxite	≤75

characterized using X-ray Diffractometer (XRD), Fourier Transform InfraRed (FTIR), X-ray spectroscopy (EDX), Scanning Electron Microscopy (SEM), UV–vis Spectroscopy and Porosimetry methods to provide information on the pore distribution. Zn doped zeolite were then prepared from the synthesized zeolitic materials through ion exchange technique. The adsorption of dye molecules onto Zn-zeolite were then examined using methylene blue.

2. Materials and methods

2.1. Materials

NaOH, zinc acetate dehydrate pellets and methylene blue dye were obtained from Sigma Aldrich, London, United Kingdom (UK), Kaolin from Kibi, Feldspar from Akyem Akroso, and Quartz from Akwatia all in the Eastern region of Ghana and also, Bauxite from Ghana Bauxite Co. in the Western region of Ghana.

2.2. Synthesis of zeolites

Particle size analysis was done on the kaolin (Kb), bauxite (Bx), feldspar (Fd) and silica (Si) samples with the aid of Retsch-VS1000 mechanical shaker with ≤75 μm sieve arrangement to get a fine particle size distribution (Table 1) and also, to remove any foreign particle and impurities present in the samples. Batch composition with respect to wt% kaolin (Kb), bauxite (Bx), feldspar (Fd) and silica (Si) were each measured into separate crucibles using a Cole Palmer made electronic balance. The different batch formulations made are summarized in Table 2. Calcination of the samples were done at a temperature of 600°C to convert the kaolin, bauxite, feldspar and silica into a more reactive phases. This was followed by reaction of the composition with a 2 M NaOH solution in solid-to-liquid (S/L) ratio of 10 g/50 mL. The mixtures were stirred using a magnetic stirrer for 30 min to give a homogeneous mixture. The samples were allowed to age for six days followed by oven crystallization at a temperature of 100°C for 3 and 7 h. The samples were filtered and washed with excess deionized water to reduce the alkalinity of the sample after which the pH of the filtrates were measured. The samples were then placed in an oven and dried at 60°C overnight. The dried and caked samples were crushed and grinded in a mortar with a pestle to obtain fine powder for characterization.

2.3. Synthesis of zinc exchanged Zeolite A (Zn-Zeolite A)

Four grams of zinc acetate dehydrate was dissolved in 50 mL of distilled water. This was followed by adding 2 g of the as-synthesized zeolite into the solution. The mixture was then stirred continuously for 20 h to allow for ion exchange. The mixture was treated with 50 mL 0.1 M aqueous solution of NaOH for the precipitation of the zinc ions. This lasted for a period of 30 min. The precipitate was filtered and washed extensively with deionized water to remove the remaining zinc acetate. After the washing process, the residue was dried in an oven at 50°C overnight. The dried sample was again treated with 50 mL 0.1 M NaOH for another 30 min at room temperature. The sample was then filtered and dried at 60°C overnight. Finally, the dried sample was calcined in a furnace at 500°C for 2 h.

2.4. Adsorption experiments

Two milligrams/per liters aqueous solution of Methylene blue (MB) was prepared using 2 mg of MB powder in 1 L of deionised water. The resultant stock solution was diluted to obtain the batch concentrations for all adsorption experiments. The batch adsorption experiment was generally carried

Table 2. Sample designation

Samples	Designation	Crystallization time (h)
100wt% Kb	C-3	3
100wt% Kb	C-7	7
20wt% Bx +80wt% Kb	B20–3	3
20wt% Bx +80wt% Kb	B20–7	7
60wt% Bx +40wt% Kb	B60–3	3
60wt% Bx +40wt% Kb	B60–7	7
20wt% Fd +80wt% Kb	F20–7	7
60wt% Fd +40wt% Kb	F60–7	7
20wt% Si +80wt% Kb	S20–7	7
60wt% Si +40wt% Kb	S60–7	7

out with Zn-exchanged Zeolite A loading of 20 mg, at pH of 9 and in room temperature of 25°C. During the batch adsorption experiments, 60 mL of MB solution was added to the 20 mg of Zn-exchanged Zeolite A adsorbent and stirred for 2 min. Set of data was collected over a period of 0–180 min, whereby aliquots of samples were taken at 0, 10, 20, 25, 30, 50, 60, 90, 150 and 180 min. Samples were taken at these time intervals and the extracted samples were centrifuged using a micro centrifuge at 5,000 rpm for 5 min. The supernatant was then extracted using a micropipette and the absorbance measured using the Genesys 10S UV–vis spectrophotometer at the MB characteristic monochromatic wavelength (λ_{max}) of 665 nm.

Generally, pH is an important parameter in the batch adsorption study as it is capable of influencing the adsorption/ desorption process through changes in the surface charge distribution of adsorbents used (Li et al., 2013). Desorption of MB molecules from adsorbent in alkaline medium is attributed to excess OH^- in solution that are capable of competing with active sites of cationic MB molecules leading to a desorption of MB from Zn-exchanged Zeolite A through ion exchange (Fil, Ozmetin, & Korkmaz, 2012; Zhang, Li, He, Zhan, & Liu, 2013). The regeneration of used Zn-exchanged Zeolite A experiments was conducted by pH variation method. The spent Zn-exchanged Zeolite A were washed in basic medium with varying pH values of 9, 11, 12, and 13. All the batch adsorption experiments were carried out in triplicate and the average values were reported in order to minimise the random experimental and systematic errors. The data obtained from the adsorption tests were then used to calculate the adsorption capacity, q_t (mg/g) (from Equation (1)), of the adsorbent by a mass–balance relationship, which represents the amount of dye adsorbed per unit weight of zeolite, mg/g.

$$\text{Adsorption capacity, } q_t = \frac{(C_o - C_t)}{W}V \tag{1}$$

where, C_o = Dye concentration at time, $t = 0$ (mg/L), C_t = Dye concentration at time, $t = t$ (mg/L), V = volume of MB solution (mL), W = mass of Zn-exchanged Zeolite A adsorbent used (mg).

Initially, a calibration curve between the measured absorbance values at λ_{max} = 665 nm and concentrations of stock MB solution was established. This enabled a quick estimation of the MB concentrations.

2.5. Adsorption kinetics

Suitability of using low cost readily available adsorbent to design systems for industrials application can be studied through the mechanism of adsorption. Successful application of adsorption demands innovation of cheap, easily available and abundant adsorbents of known kinetic parameters and sorption characteristics. Adsorption kinetics can be modelled by several models including the

pseudo-first-order Lagergren equation and pseudo-second-order rate equation given below in non-linear forms (Qiu et al., 2009). The pseudo-first order kinetic model after integration and inserting necessary boundary conditions is given by Equation (2).

$$\log\left(q_e - q_t\right) = logq_e - \frac{k_1}{2.303}t \tag{2}$$

where, q_t is the amount of adsorbate adsorbed at time t (mg/g), q_e is the adsorption capacity at equilibrium (mg/g), k_1 is the pseudo-first-order adsorption rate constant (min^{-1}), and t is the adsorption contact time (min). The pseudo-second order kinetic model after integration and inserting necessary boundary conditions is given by Equation (3) as:

$$\frac{t}{q_t} = \frac{1}{k_2 q_e^2} + \frac{t}{q_e} \tag{3}$$

where k_2 is the pseudo-second order rate constant (g mg^{-1} min^{-1}).

2.6. Equilibrium adsorption isotherms

Adsorption isotherm represents the equilibrium relationship between the amount of adsorbate in adsorbent and solution phases. In addition, it is also useful in determining the affinity of an adsorbate for a particular adsorbent as well as estimating its adsorption capacity. Two different isotherm models were investigated for representing the adsorption data and these includes the Langmuir and Freundlich Isotherms.

Langmuir isotherm is the most simple and useful isotherm for physical and chemical adsorption types. This isotherm model assumes a homogeneous surface with no interaction between adsorbate molecules, presence of dynamic equilibrium between adsorption and desorption, and the maximum adsorption assumed to be of a monolayer (Vafajoo, Ghanaat, & Ghalebi, 2014). The saturated monolayer isotherm model can be expressed in Equation (4):

$$q_e = \frac{Q_m K_L C_e}{1 + K_L C_e} \tag{4}$$

The linearized form of Equation (4) becomes:

$$\frac{C_e}{q_e} = \frac{1}{Q_m K_L} + \frac{C_e}{Q_m} \tag{5}$$

where Q_m is maximum adsorption capacity at monolayer (mg/g), K_L is the Langmuir adsorption constant (L/mg) related to the binding sites affinity and energy of adsorption, C_e is the equilibrium concentration of the adsorbate.

It is well known that the separation factor (R_L) is crucial in determining the suitability of Langmuir isotherm model to model the adsorption process (Fil et al., 2012; Yan, Wang, Yao, Zhang, & Liu, 2009) A value of $0 < R_L < 1$ indicates that it is a favourable adsorption process, while $R_L > 1$ shows that it is an unfavourable adsorption, $R_L = 1$ means linear adsorption, and $R_L = 0$ signifies irreversible adsorption. R_L can be estimated mathematically from Equation (6):

$$R_L = \frac{1}{1 + K_L C_o} \tag{6}$$

where R_L is the separation factor (dimensionless), K_L is the Langmuir adsorption constant (L/mg), C_o is the initial concentrations of MB (mg/L).

On the other hand Freundlich isotherm is an empirical equation that is derived by assuming a heterogeneous surface with a non-uniform distribution of the heat of adsorption over the surface of adsorbent and it can be represented by Equation (7):

$$q_e = K_F C_e^{\frac{1}{n_f}} \tag{7}$$

The linearized form of the Equation (7) is:

$$lnq_e = lnK_F + \frac{1}{n_f} lnC_e \tag{8}$$

where K_F (mg/g) (L/mg) $^{(1/n_f)}$ is the Freundlich constant related to the bonded energy and n_f is the heterogeneity factor. Here, n_f measures the degree of linearity of adsorption.

2.7. UV–vis spectroscopy

Adsorption of the methylene blue molecules onto Zn-exchanged zeolites was monitored using UV–vis spectroscopy. The sample was scanned between 200 and 900 nm wavelengths in a GENESYS 10S UV–vis (version v4.005 2L5S048209). Characteristic peak of methylene blue at 665 nm wavelength was observed and the corresponding absorbance measured to extract the corresponding concentration from a calibration curve.

2.8. X-ray fluorescence

AMETEX USA Spectro XLab 2000 X-ray Fluorescence (XRF) was used to analyse the chemical composition of all the raw material deposits. Four grams of each sample was mixed with 1 g of Licowax powder that served as a binder. The samples were then milled in a Restch Milling machine and pressed before loading into the Spectro Xlab 2000 for analysis.

2.9. X-ray Diffraction

Powder XRD patterns were recorded using the Empyrean PANalytical series 2 XRD with CuKα (1.54Å) radiation source and a tube operating at 40 mA and 40 kV. The phases in the samples were identified using X'Pert Highscore plus database software.

2.10. FTIR spectroscopy

In this work Attenuated Total Reflectance (ATR) was employed with single bounce diamond anvil ATR accessory fitted to a Thermo-Fisher Nicolet IS50 FT-IR spectrometer.

2.11. Porosimetry

The porosity and surface area were measured using Quantochrome NOVA 4200e instrument by N_2 adsorption using Novawin v11.0 analysis software. Sample was degassed under vacuum at 120°C for 24 h prior to analysis. Adsorption and desorption isotherms were recorded at −196°C.

2.12. SEM and energy dispersive EDX

The structural morphology and empirical elemental compositions were estimated using energy dispersive EDX-Zeiss EVO LS10 SEM equipped with Oxford INCA X-act detector.

3. Results and discussions

3.1. X-ray fluorescence

XRF analyses were done on all the raw materials to determine the percentage composition of all the oxides present in the raw materials. From Table 3, it can be observed as expected that Quartz represents the highest silica source followed by feldspar, and kaolin with the least being bauxite. Quartz and Feldspar are therefore very high silica sources and were used in varying the Si/Al ratio of the as-synthesized zeolite. As presented in Table 3, Bauxite had the highest percentage of alumina and

was used as the Al source to vary the Si/Al ratio of the as-synthesized zeolite. In addition, Kibi Kaolin and Awaso Bauxite have relatively high Fe_2O_3 content. These observed differences in mineral composition suggest that the batch formulations will play a key role in the type of zeolites formed.

3.2. X-ray diffraction

XRD analysis was done on the unheated kaolin in order to compare the phases present with that of metakaolin (calcined kaolin). Figure 1 depicts the XRD pattern for the raw kaolin and the calcined kaolin.

The XRD pattern of the Kibi kaolin in Figure 1(b) shows an intense peak position at $2\theta = 24.88°$. The position of the kaolinite phase at $2\theta = 24.88°$ is related to the characteristic X-ray diffraction peak of kaolinite reported at $2\theta = 24.64°$ (Gougazeh & Buhl, 2014) confirming that the sample used was kaolin. Again from Figure 1(a), it can be observed that upon calcination, the crystalline peaks of the kaolin disappeared with the formation of a more amorphous metakaolinite phase with a reduction in the degree of crystallinity.

Figure 2(a–c) shows the XRD pattern of 3 samples crystallized for 3 h. With reference to Figure 2(a and b), it is observed that for Figure 2(a) (B60–3) iron oxide forms, while for Figure 2(b) (B20–3 designation), hematite was formed. The zeolite phase had not begun crystallizing for these two samples while for the control experiment (Figure 2(c)), the zeolite phase had begun crystallizing. The diffraction pattern for the controlled experiment (Figure 2(c)) with the 2θ peak positions of 19.3°, 25.3°, and 30.6° was matched with that in literature and was identified to be zeolite ITQ-7 (Siliceous, Calcined) with a chemical formula $Si_{64}O_{128}$. The ITQ-7 (Siliceous, Calcined) has a tetragonal crystal structure (Baerlocher, McCusker, & Olson, 2007). This suggests that the crystallization time of 3 h was not enough for the crystallization of the zeolite phase in the batch formulations containing bauxite.

The XRD pattern for the control experiment (C-7) together with samples with bauxite formulations (B20–7 and B60–7) and calcined for 7 h are shown in Figure 3. The XRD patterns of B60–7 and B20–7 are presented in Figure 3(a) and (b), respectively. The B60–7 and B20–7 were identified and matched as Zeolite A, (Na) and Zeolite A, (Na dehydrated), respectively. Both recorded major peaks at 2θ: 7.1, 10.1, 12.4, 16.1, 21.6, 24, 26.1, 27.1, 29.9, and 34.1°. The compound name and chemical formula of Zeolite A (Na) is given as Sodium Aluminum Silicate Hydrate ($Na_{96}Al_{96}Si_{96}O_{384}{\cdot}216H_2O$) and Zeolite A (Na, dehydrated) is given as Sodium Aluminum Silicon Oxide Hydrate and $Na_{92.70}$ ($Si_{96.96}Al_{95.04}O_{384}$) $(H_2O)_{6.95}$. The diffraction pattern of the control experiment, C-7 (crystallization for 7 h) identified in Figure 3(c), was matched with that of literature (Treacy & Higgins, 2001) and this was identified to be of Zeolite A with Linde Type A (LTA) structure. The 2θ peak positions of the as-synthesized zeolite corresponded with that of Zeolite LTA. All the three as-synthesized zeolites have cubic crystal structure.

The XRD pattern for the F60-7 and F20-7 as presented in Figure 4(a and b) correspond respectively to Zeolite A (K-exchanged, dehydrated) and Zeolite A. Zeolite A (K-exchanged, dehydrated) has the chemical formula of $Al_{12}K_{12}O_{48}Si_{12}$ and that of Zeolite A is $H_2Al_{12}N_{10}Na_{22}O_{79}Si_{12}$. Both zeolite types have the cubic crystal structure. Also, the XRD patterns of the samples varied with raw silica addition i.e. S20-7 and S60-7, identified in Figure 5(a and b) was matched using X'pert Highscore Plus database software. They both matched Zeolite A with mixed minor phases of zeolite SSZ-44 ($Si_{32}O_{64}$) with a monoclinic crystal structure.

Table 4 shows a summary of the batch formulations, process conditions and the zeolites formed. It can be seen that 7 h of calcination time resulted in the formation of Zeolite A with structural variations depending on the Si/Al concentration in the batch formulations.

To analyze the effect of the compositional variation on the as-synthesized zeolites, the crystallite sizes of the synthesized zeolites were computed based on the Scherer's equation (Equation (9)) at a 2θ position of 29.9°, wavelength, $\lambda = 0.154$ nm and a shape factor, K = 0.94.

Table 3. XRF analyses of raw materials

Raw materials	Si_2O	Al_2O_3	Na_2O	MgO	P_2O_5	SO_3	Cl	K_2O	CaO	TiO_2	MnO	Fe_2O_3	L.O.I	Total
Kaolin	48.91	20.49	0.82	0.84	0.16	0.21	0.04	0.81	0.02	0.87	0.01	11.73	14.6	99.51
Feldspar	70.57	12.6	3.6	1.26	0.06	0.05	0.15	10	1.2	0.03	0.01	0.33	0.16	100.02
Quartz	96.84	0.11	0.54	2.08	0.05	0.05	0.14	0.11	0.01	0.02	0.00	0.03	1.06	101.04
Bauxite	2.75	65.15	1.05	0.08	0.15	0.13	-	0.04	0.06	1.93	0.01	6.99	23.08	101.42

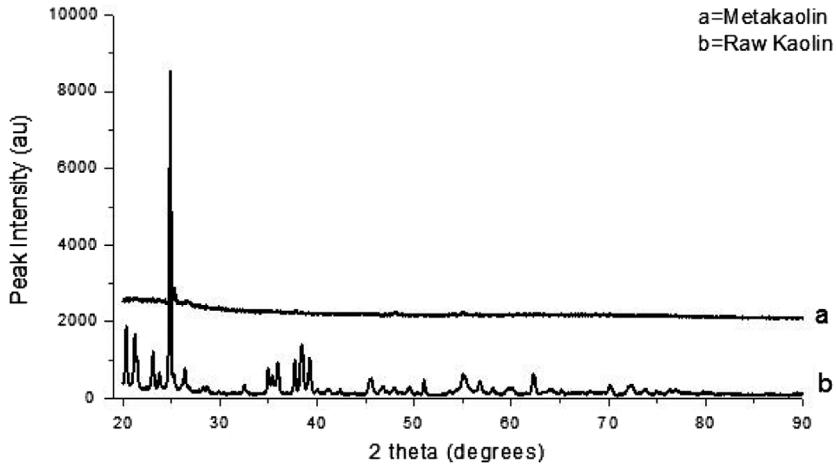

Figure 1. XRD Pattern for Kaolin and Metakaolin.

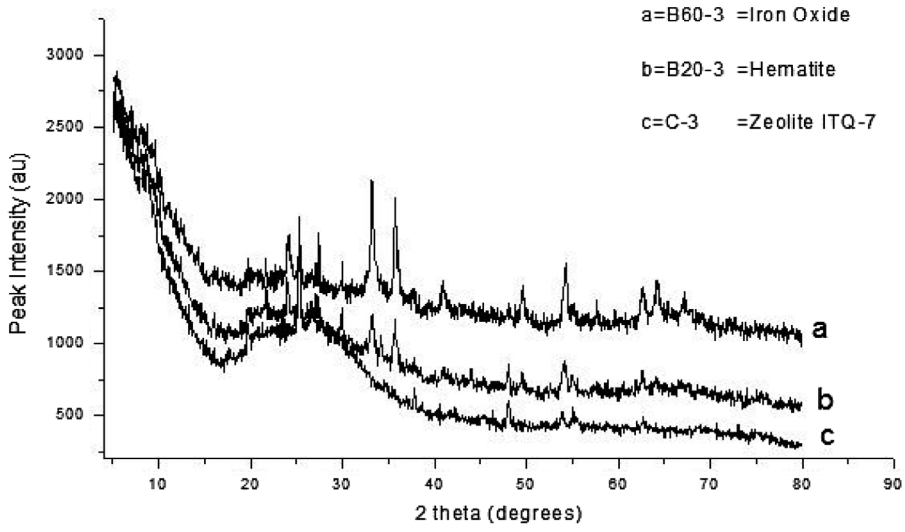

Figure 2. The XRD pattern for the samples crystallized for 3 h (for batch formulations containing bauxite).

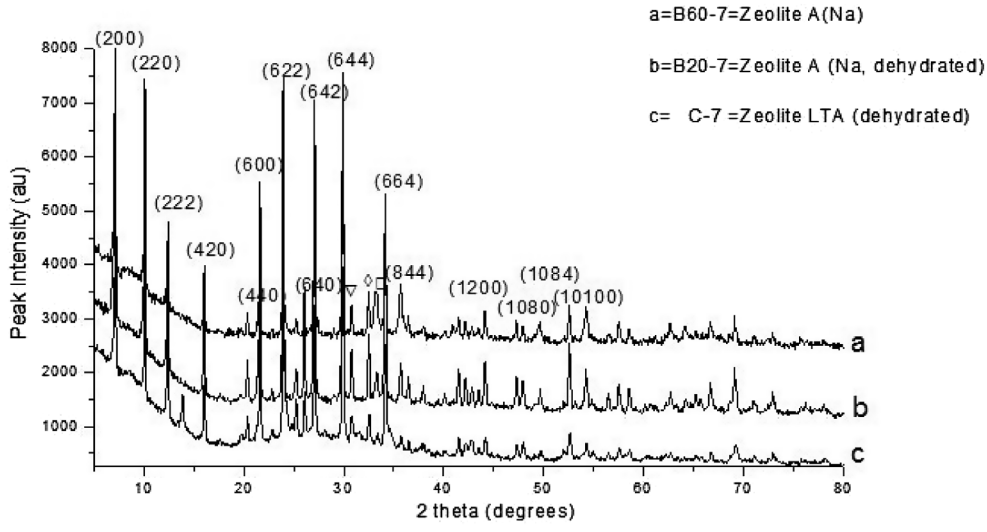

Figure 3. XRD pattern of the control experiment with the as-synthesized zeolite varied with bauxite addition.

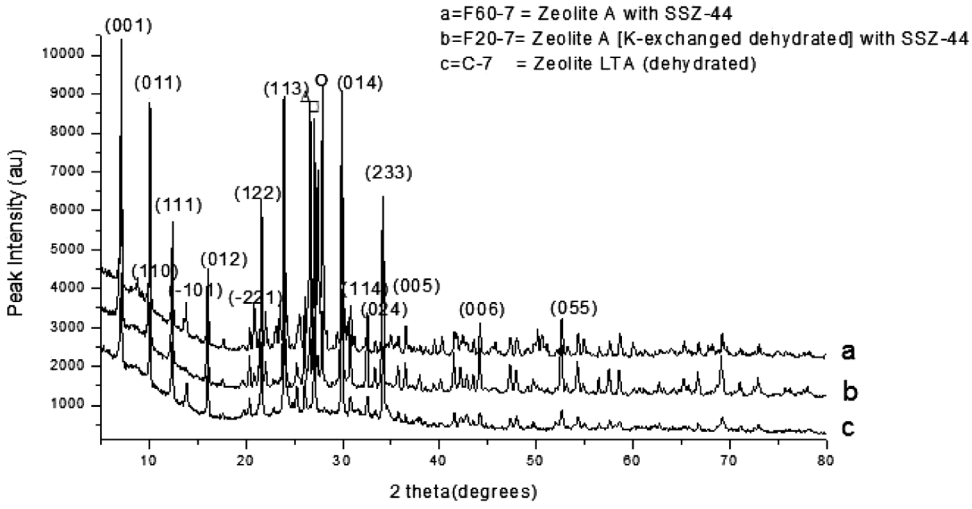

Figure 4. XRD pattern of the control experiment with the as-synthesized zeolite varied with feldspar addition.

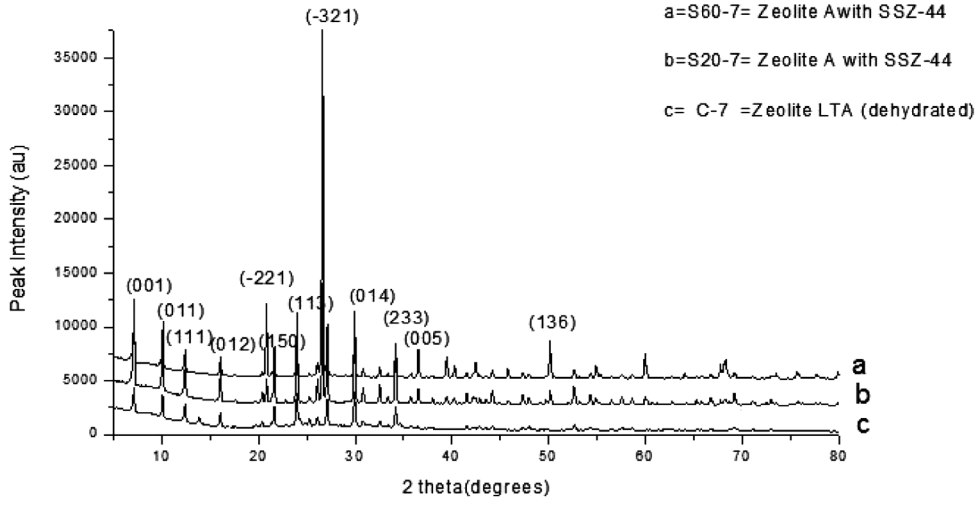

Figure 5. XRD pattern of the control experiment with the as-synthesized zeolite varied with raw silica addition.

The Scherer's equation is given below;

$$L = \frac{0.94\lambda}{\beta cos\theta} \tag{9}$$

where λ = wavelength of X-ray (Cu Kα), β = Full width at Half Maximum, θ = Bragg's Angle, L = crystallite size.

From the computed crystallite sizes, it was observed that the crystallite size of the control experiment (C-7) was 34 nm however, after adding feldspar which is a silica source, the crystallite sizes increased to 43 and 51 nm for samples F20-7 and F60-7, respectively. When raw silica which has relatively higher silica content than feldspar was added, the crystallite size was recorded as 48 and 51 nm, respectively for S20-7 and S60-7. This suggested that the crystallite size of the synthesized zeolite generally increased with increasing Si content (Si/Al ratio) confirming reported works that the degree of crystallinity increases with increasing crystallite sizes (Kiricsi, Pál-Borbély, Nagy, & Karge, 1999). Also, with the addition of 20 wt% bauxite (B20-7) to the raw kaolin, the crystallite size changed from 34 nm (C-7) to about 43 nm. Upon increasing the bauxite content to 60 wt%, there was a decrease in crystallite size from 43–36 nm. This indicates clearly that the amount of Silica/Alumina

Table 4. Process conditions and XRD results of synthetic zeolites

Batch no.	S/L (g/ml)	Agitation (h)	Aging time (d)	Crystallization time (h)	XRD results
C-3	10/50	0.5	6	3	ITQ-7 (Sil., Calcined)
B20–3	10/50	0.5	6	3	-
B60–3	10/50	0.5	6	3	-
C-7	10/50	0.5	6	7	Zeolite A (Hyd.)
F20–7	10/50	0.5	6	7	Zeolite A (K exch. Dehyd.) +SSZ-49
F60–7	10/50	0.5	6	7	Zeolite A+SSZ-49
S20–7	10/50	0.5	6	7	Zeolite A+SSZ-49
S60–7	10/50	0.5	6	7	Zeolite A+SSZ-49
B20–7	10/50	0.5	6	7	Zeolite A (Na, dehyd.)
B60–7	10.0/50.0	0.5	6	7	Zeolite A (Na)

Notes: S/L = Solid-to-Liquid ratio, Exch. = Exchanged, Sil. = Siliceous, LTA = Linde Type A.

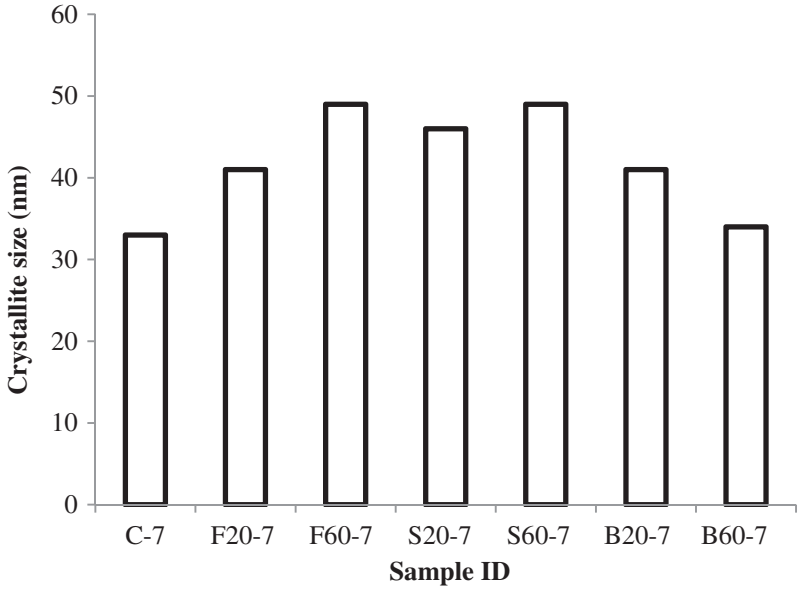

Figure 6. The effect of varying the Si/Al on the crystallite sizes.

present in the formulations has a significant effect on the Si/Al ratio as well as the degree of crystallinity and the crystallite size formed. It has been reported that increasing Si/Al ratio leads to a remarkable improvement in the physical properties of zeolites and this can be exploited in several commercial applications (Nazila, Hossein, & Dariush, 2011). Furthermore, by comparing the samples crystallized for 3 and 7 h, it was observed that zeolite phase crystallized better for the longer crystallization time (7 h) as compared with the shorter crystallization time (3 h) indicating that crystallization increases with crystallization time as observed in this work. In Figure 6, the effect of the batch formulations is shown graphically.

3.3. Fourier transform infra-red

FTIR spectroscopy is used to specify the structure of zeolites and to monitor reactions in the zeolite framework. This spectrum can also be used to indicate the secondary building units of zeolitic structures such as double rings and pore opening (Kiricsi et al., 1999). The FTIR spectra for the control experiment (C-7) with the synthesized zeolite samples varied with 20 and 60 wt.% of bauxite, feldspar and silica are represented in Figures 7 and 8 respectively.

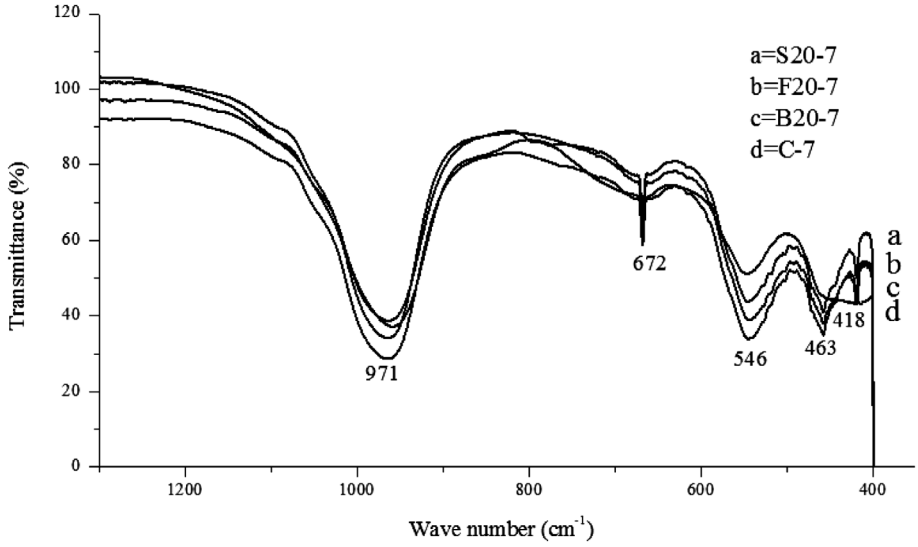

Figure 7. The FTIR of the control experiment and the synthesized zeolite samples containing 20 wt.% of bauxite, feldspar and silica respectively.

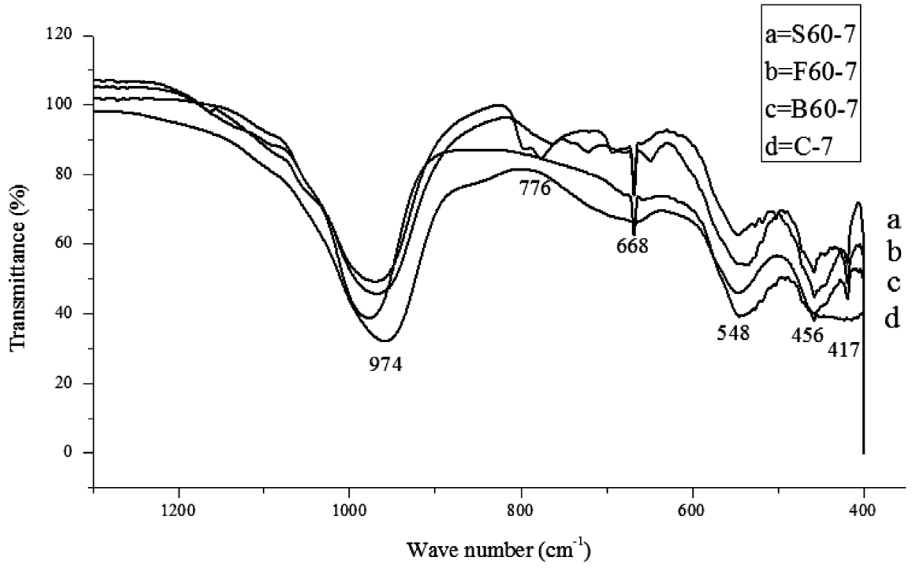

Figure 8. The FTIR of the control experiment and the synthesized zeolite samples containing 60 wt.% of bauxite, feldspar and silica, respectively.

In the spectral range of 1,500–200 cm^{-1}, information about the vibration frequencies in zeolites can be obtained (Lesničenoks, Grīnberga, & Kleperis, 2014). The spectra at position 957, 965,979, 970, 971, 975 cm^{-1} found between 1,250 and 950 cm^{-1} and the spectral 662, 665, 667,668, 672, 695 cm^{-1} found between 720 and 650 cm^{-1} indicate internal vibrations due to asymmetric stretching and internal vibrations due to symmetric stretching, respectively. Also, the bands 547,544, 545, 550, 541, 546, and 548 cm^{-1} found within the band range of 650–500 cm^{-1} of the as-synthesized zeolite samples represent the external T-O linkage (*T* = Si or Al) due to double ring. Consequently, the presence of internal tetrahedron vibrations of Si–O and Al–O of sodalite (T–O–T) with bending modes of the sodalite framework found in zeolites corresponds to the spectra at position 456, 459, 460, 462, and 463 cm^{-1} found within the spectral zone of 500–420 cm^{-1} of the as-synthesized zeolite samples (Gougazeh & Buhl, 2014). Finally, information on the external T-O linkage due to the pore openings found in zeolite was obtained as a result of bands found at 420 cm^{-1}, 418 cm^{-1}, 417 cm^{-1}, and 416 cm^{-1} which are found between the spectral zone of 420–300 cm^{-1} (Gougazeh & Buhl, 2014; Jacobs & Uytterhoeven, 1972; Lesničenoks et al., 2014). These obtained spectral vibrations indicate the formation of zeolitic structure.

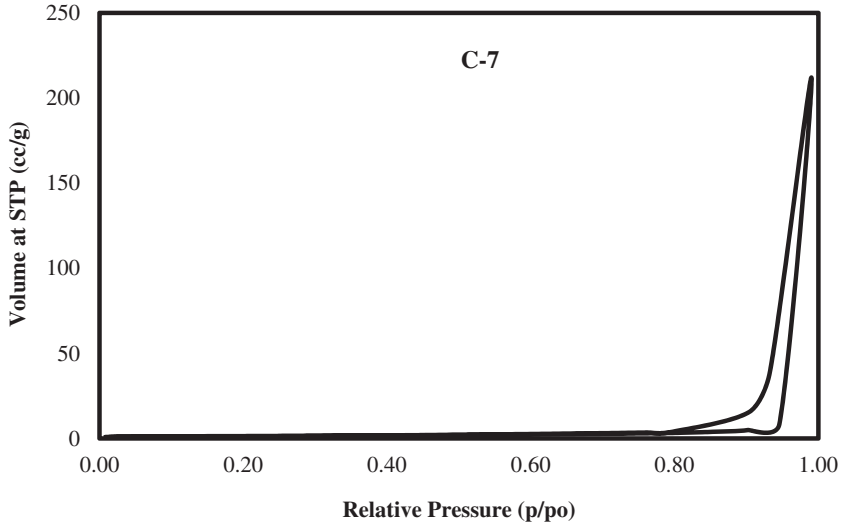

Figure 9. The N_2 adsorption/ desorption isotherm of synthesized zeolite (Control experiment, C-7) nanoparticles.

3.4. Porosimetry

The adsorption/desorption isotherm curves of N_2 at normal boiling temperature was used for studying the BET surface area, pore diameter and pore volume of the synthesized zeolite. The graph in Figure 9, represents the N_2 adsorption/desorption isotherm of the synthesized zeolite for the control experiment C-7. This shows an isotherm characteristic of multi-porous materials (mixed micro and meso porous) thereby confirming the porous framework of the zeolites.

3.5. Scanning electron microscopy

SEM imaging was performed to examine the textural properties of the zeolites to confirm the XRD results. In Figure 10, the as synthesized zeolite A is observed to exhibit cubic crystal structure with no agglomeration of particles. The observed cubic crystal structure from the SEM image in Figure 10(a) confirms the XRD analysis which suggests the formation of zeolite A with LTA structure. Figure 10(b)

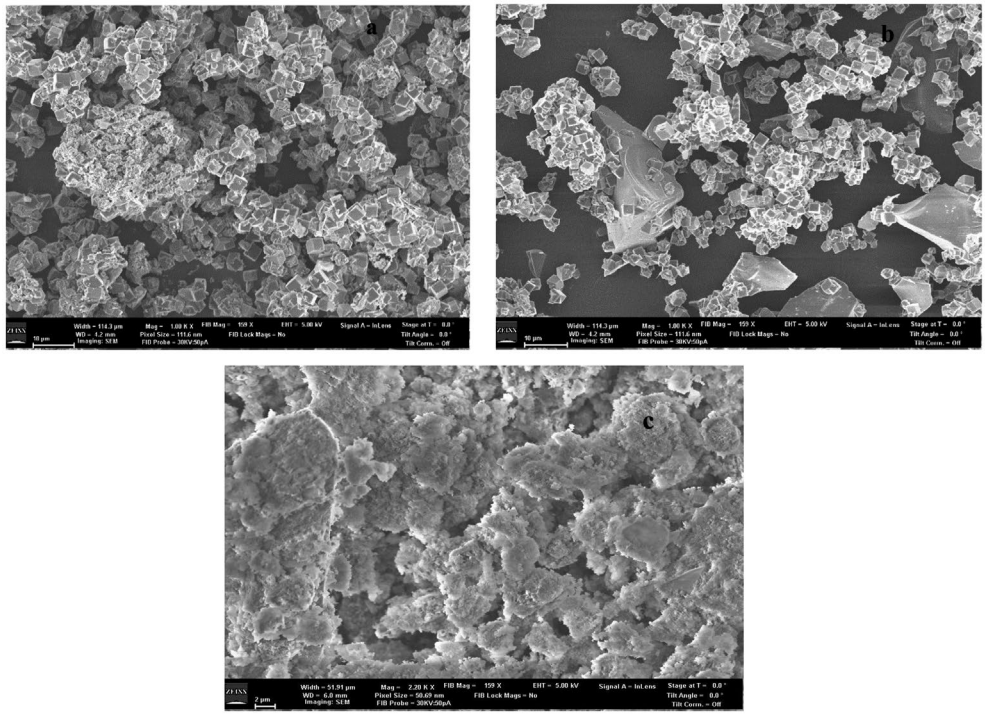

Figure 10. SEM of (a) Zeolite A; (b) SEM of Zeolite A formulated with 60% Silica; (c) SEM of Zn exchanged Zeolite A.

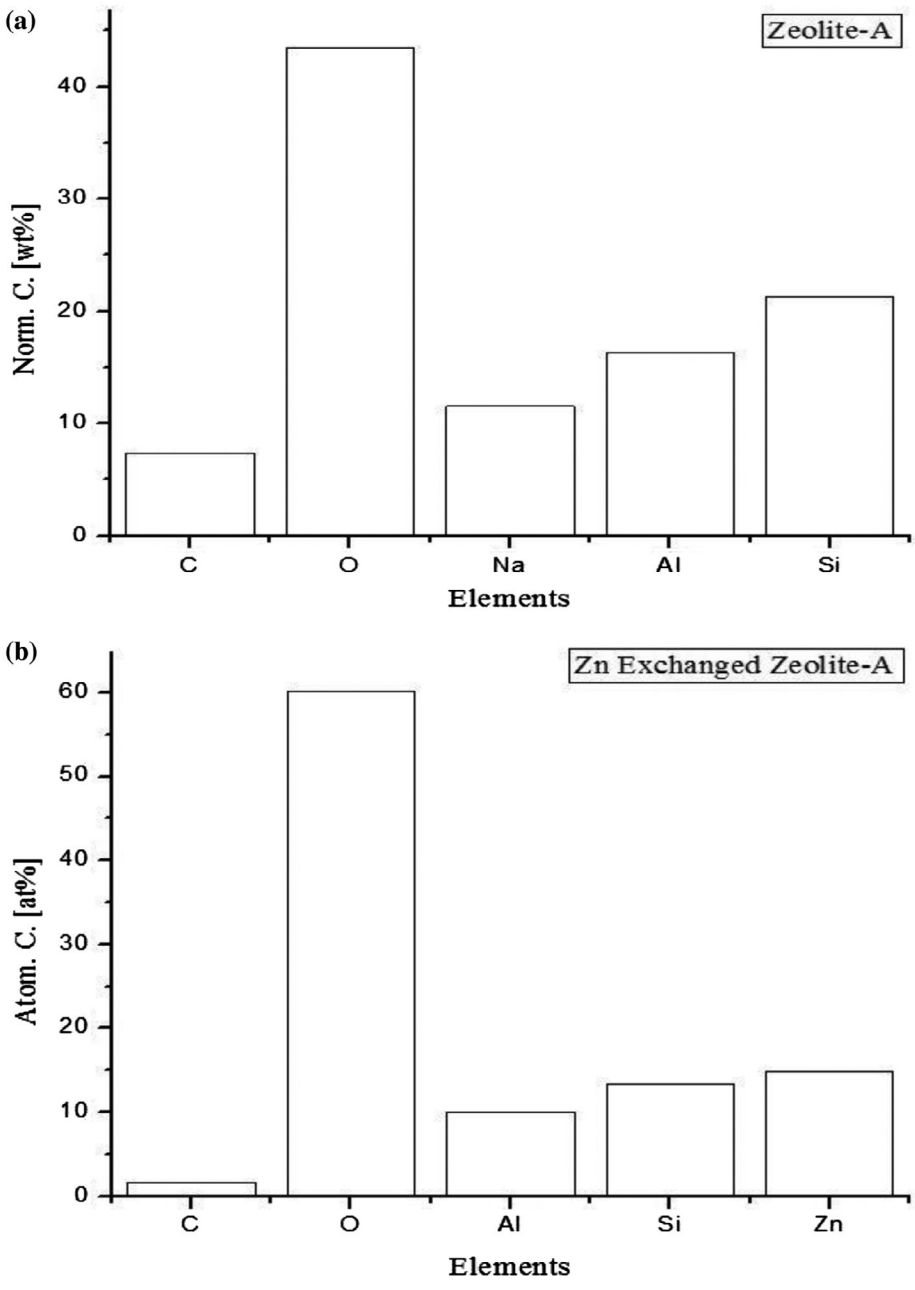

Figure 11. EDX of (a) Zeolite-A; EDX of (b) Zn exchanged Zeolite-A.

shows a morphology similar to Figure 10(a). This observation suggests that the batch formulation did not affect the morphology of the zeolites with a silica content as high as 60%. In Figure 10(c), some form of structural complexes took place during the Na and Zn ion exchange process. This is of great interest for further investigations since the morphological changes is capable of impacting on the composite's efficacy for potential applications.

3.6. Energy dispersive X-ray analysis

EDX was carried out to examine the elemental distribution in the zeolite framework. Figure 11 shows the elemental mapping. In Figure 11(a), it can be seen that Si/Al is approximately 1 indicating that the as synthesized zeolite is Zeolite A with Na as the cation balancing the negative framework of $[AlO_4]^{5-}$ and $[SiO_4]^{4-}$. In Figure 11(b) it can be seen that Na completely disappear from the elemental

Figure 12. Absorbance intensity curve at various time interval.

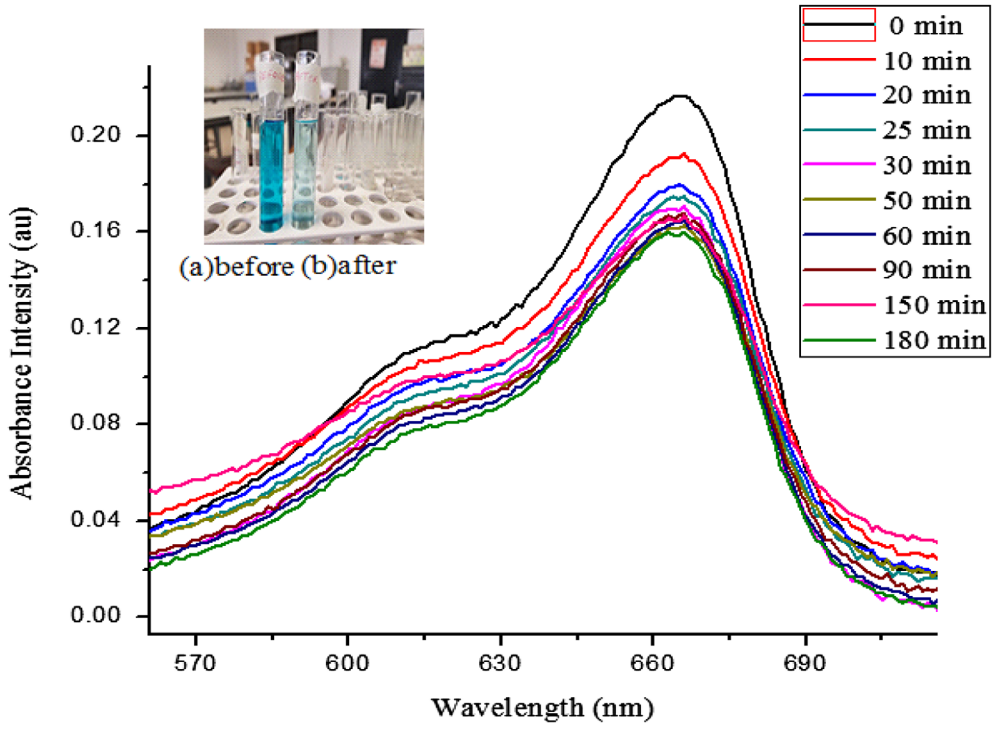

spectra. Zinc is however mapped, indicating successful ion exchange between Na and Zn and encapsulation of zinc based nanocatalyst in the zeolite framework.

3.7. Zn-exchanged zeolite A adsorption studies

The feasibility of the synthesized Zn Exchange zeolite A to adsorb Methylene blue from solution was examined through adsorption kinetics studies which is very necessary in order to depict the features of adsorbent. The effect of contact time on adsorption of MB onto the Zn-exchanged Zeolite A samples are shown in Figure 12. It can be seen that the adsorption of MB onto Zn-exchanged Zeolite A and adsorption equilibrium was approximately reached within 180 min.

To investigate the mechanism and characteristics of adsorption, MB adsorption kinetics on Zn-exchanged Zeolite A samples were fitted by pseudo-first-order model and pseudo-second-order using Equations (2) and (3) and depicted in Figure 13(a) and (b) respectively. From values of correlation coefficients from the fitted graphs in Figure 13(a) and (b), the adsorption kinetics of the MB onto Zn-exchanged Zeolite A is of pseudo-second-order model with $R^2 = 0.99018$ than by the pseudo-first-order model with $R^2 = 0.27355$. In addition, the calculated equilibrium adsorption capacity (q_e) from the pseudo-second-order model is 1.3089 mg/g and very close to the experimentally obtained equilibrium adsorption capacity of 1.2811 mg/g (as shown in Table 5). These results indicated that the adsorption kinetics of MB onto the Zn-exchanged Zeolite A could be well described by the pseudo second-order model suggesting that chemisorption is responsible for the overall rate of the adsorption process (Hameed, Ahmad, & Latiff, 2007; Mckay & Ho, 1999).

The Langmuir and Freundlich isotherm adsorption models (Equations (5) and (8)) were used to further study the adsorption property of Zn-exchanged Zeolite A. The fitting results for the Langmuir and Freundlich models are depicted in Figure 14(a) and (b) with the values of isotherm constants presented in Table 6 respectively. The Correlation coefficient for the Langmuir isotherm (R^2) is 0.91851 with the values of the separation factor, R_L less than one (i.e. 0.6247, 0.4516, 0.3551 and 0.2517) indicating that the adsorption process is favourable (Freundlich, 1906; Langmuir, 1918). The R^2 extracted for Freundlich isotherm is 0.96682. This value is higher than that of Langmuir model

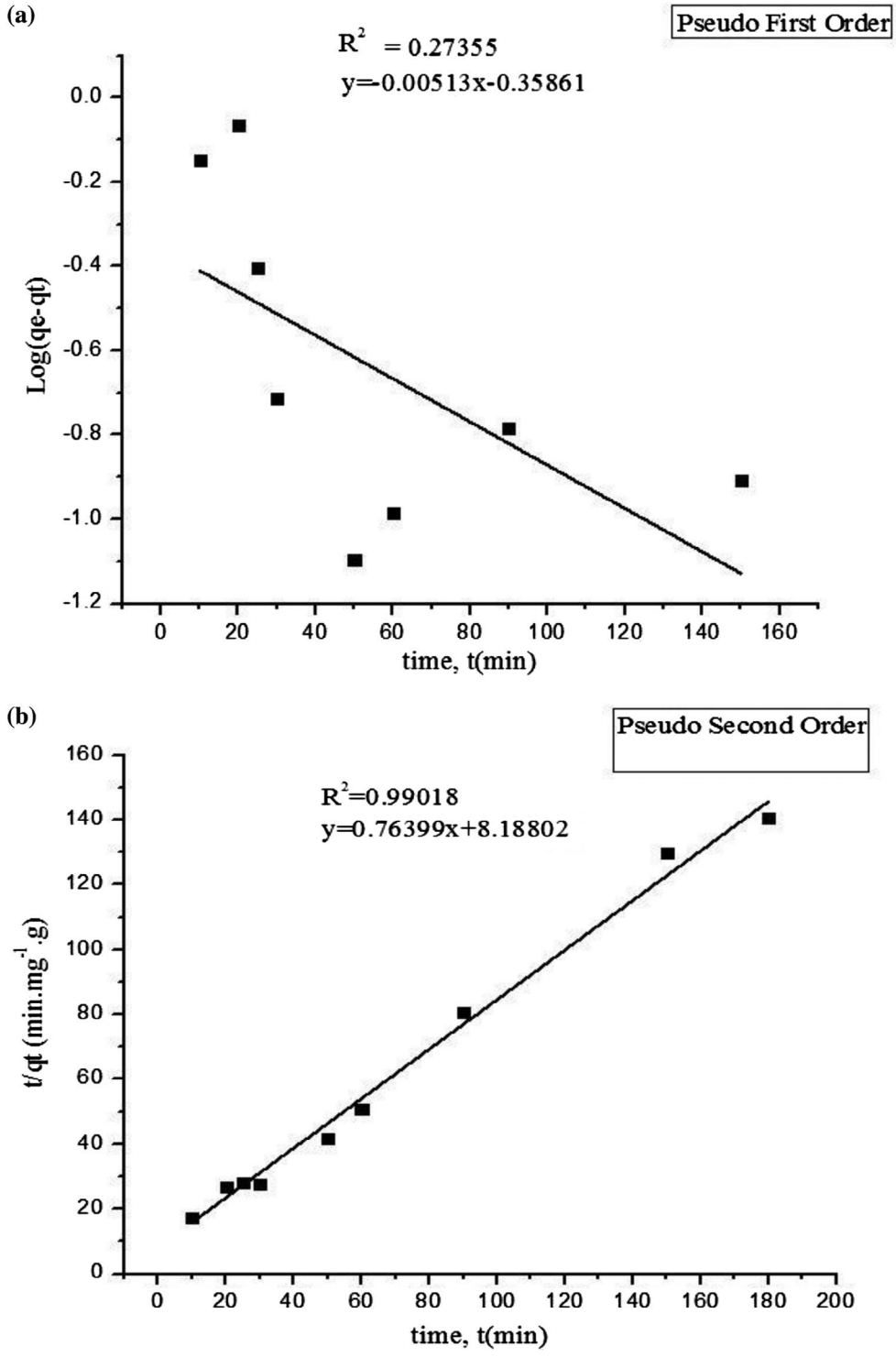

Figure 13. (a) Pseudo first-order; (b) Pseudo second-order.

Table 5. Parameters of kinetic models of MB adsorption on the adsorbent

Adsorbent	Exp.	Pseudo first order model			Pseudo second order model		
	q_e(mg/g)	k_1(min^{-1})	q_e(mg/g)	R^2	k_2(g mg^{-1} min)	q_e(mg/g)	R^2
Zn-exchanged Zeolite A	1.2811	0.011814	0.43792	0.27355	0.07128	1.3089	0.99018

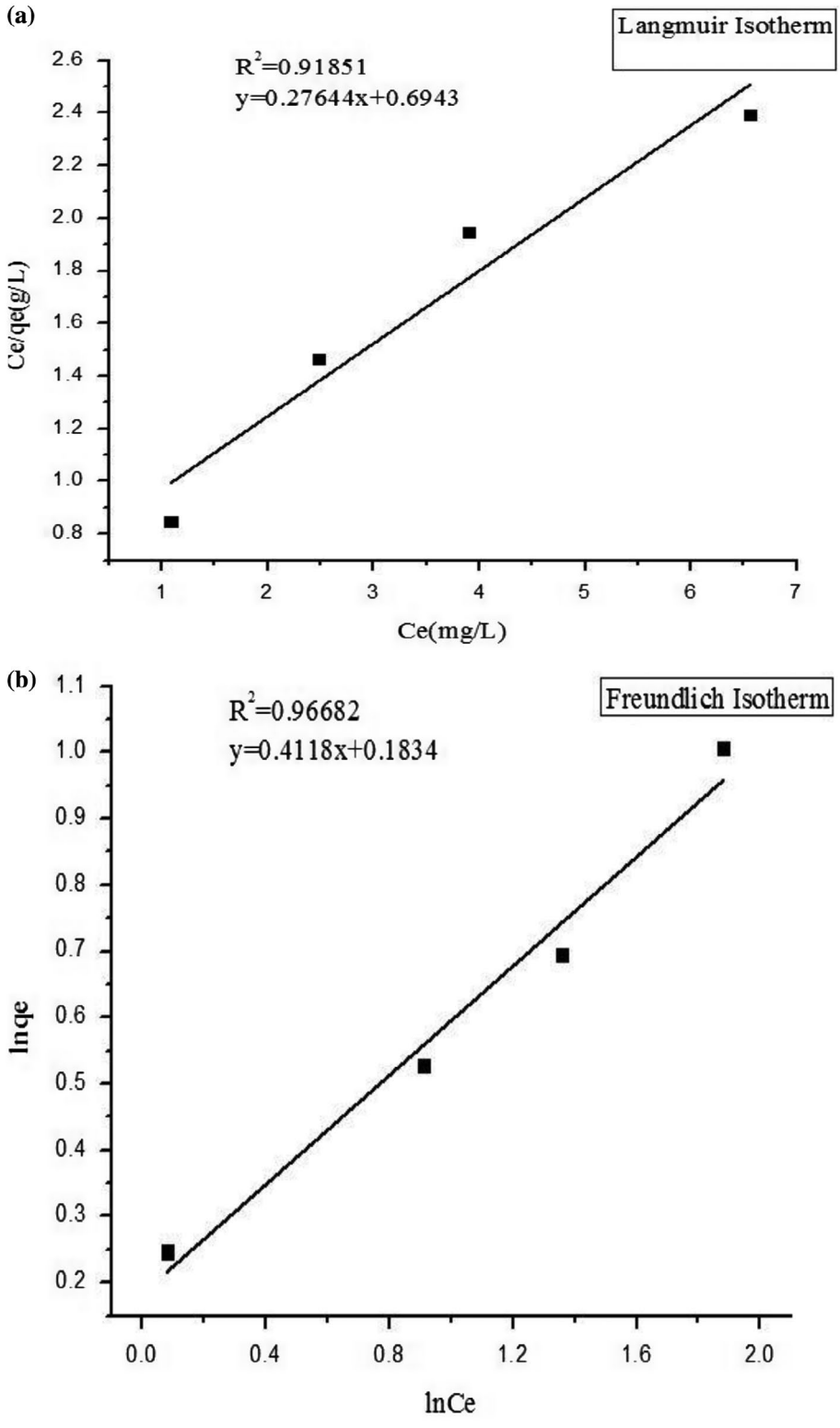

Figure 14. (a) Langmuir Isotherm model; (b) Freundlich Isotherm model.

Table 6. The adsorption isotherm parameters

Langmuir isotherm		Freundlich isotherm	
Parameter	**Value**	**Parameter**	**Value**
Q_m (mg/g)	3.61742	K_F	1.20129
K_L (L/mg)	0.39816	$1/n_f$	0.4118
R^2	0.91851	R^2	0.96682

Table 7. The regeneration performance of the alkaline treated adsorbent

pH	Intensity (a.u.) at t = 30 min	Corresponding concentration (mg/L)	Regeneration performance (%)
9	0.058	0.3949	34.44
11	0.073	0.497	43.35
12	0.080	0.5446	47.5
13	0.076	0.5174	45.12

suggesting that the Freundlich model better describes the interaction among adsorbate molecules onto the Zn-exchanged Zeolite A adsorbent. This therefore suggests a multilayer distribution of adsorbate molecules with some level of interaction between adsorbed molecules (Freundlich, 1906; Langmuir, 1918).

3.8. Regeneration studies

The results for the regeneration performance of adsorbent which were treated with different pH are tabulated in Table 7 and shown graphically in Figure 15. Regeneration of spent adsorbent depends on a number of factors such as pH, temperature, adsorbent type etc. By changing the conditions in the adsorbent it is possible to lower the equilibrium loading capacity through temperature or partial pressure variation. This suggests that the relatively low regeneration capacity recorded can be optimized through further investigation.

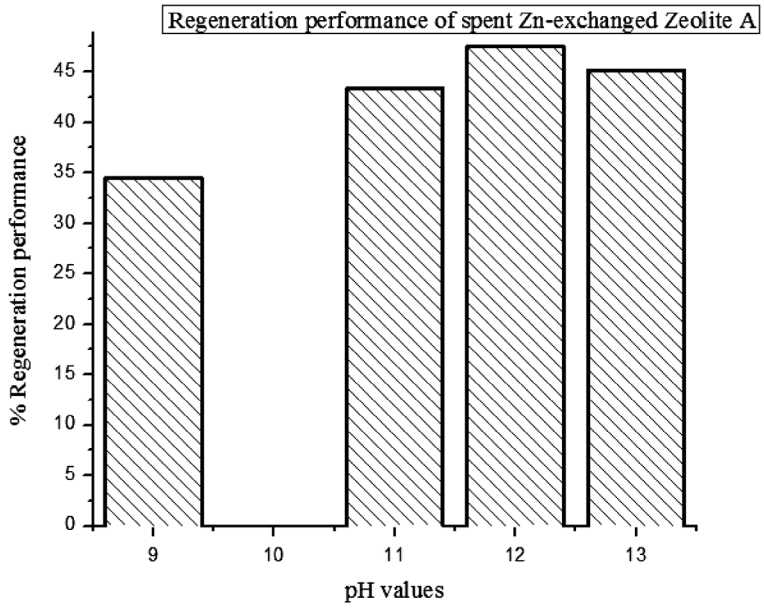

Figure 15. Regeneration of spent Zn-exchanged Zeolite A.

4. Conclusion

The potential of formulating Zeolites from natural aluminosilicate based materials for use as adsorbent has been successfully tested. The different forms of zeolites synthesized as matched by the XRD pattern include: Zeolite A (LTA, hydrated), Zeolite A (Na) and Zeolite A (Na, dehydrated), Zeolite A (K- exchanged, dehydrated). Higher crystallization time in the range of 7 h is required for the zeolite phases to be formed. Variation in the Si/Al ratio using batch formulation of the aluminosilicate based materials showed that higher silica amount in the formulations results in lager crystallite sizes while the use of higher amount of bauxite content (alumina) results in the formation of zeolites with smaller crystal sizes. Zn-exchanged Zeolite A showed reasonable adsorption for methylene blue dye molecules. The adsorption kinetics of the MB onto Zn-exchanged Zeolite A was observed to follow pseudo-second-order model. Freundlich model better described the interaction among adsorbate molecules onto the Zn-exchanged Zeolite A adsorbent, suggesting a multilayer distribution of adsorbate molecules with some level of interaction between adsorbed molecules. The regeneration capacity of the adsorbent was relatively low and calculated to be about 48% at pH of 12.

Acknowledgements
This work was supported by the Royal Society of Chemistry, Leverhulme African Award Phase II, through Professor Karen Wilson, Aston University, Birmingham, U.K. The authors will also like to thank Ghana Geological Survey for the XRF analysis on the raw materials.

Funding
This work was supported by University of Ghana [grant number UGRF10].

Author details
Emmanuel Nyankson[1]
E-mail: enyankson@ug.edu.gh
Johnson Kwame Efavi[1]
E-mail: jkefavi@ug.edu.gh
Abu Yaya[1]
E-mail: ayaya@ug.edu.gh
Gloria Manu[1]
E-mail: gpmanu@ug.edu.gh
Kingsford Asare[1]
E-mail: kings.word22@yahoo.com
Joseph Daafuor[1]
E-mail: josephdaafuor@gmail.com
Richard Yeboah Abrokwah[2]
E-mail: ryabrokw@aggies.ncat.edu
[1] School of Engineering Sciences, Department of Materials Science & Engineering, University of Ghana, P.O. BOX LG 74, Accra, Ghana.
[2] Energy and Environmental Systems Department, North Carolina A&T State University, Greensboro NC 27411, USA.

Citation information
Cite this article as: Synthesis and characterisation of zeolite-A and Zn-exchanged zeolite-A based on natural aluminosilicates and their potential applications, Emmanuel Nyankson, Johnson Kwame Efavi, Abu Yaya, Gloria Manu, Kingsford Asare, Joseph Daafuor & Richard Yeboah Abrokwah, *Cogent Engineering* (2018), 5: 1440480.

Cover image
Source: Authors.

References

Alver, E., & Metin, A. U. (2012). Anionic dye removal from aqueous solutions using modified zeolite: Adsorption kinetics and isotherm studies. *Chemical Engineering Journal, 200–202*, 59–67. doi:10.1016/j.cej.2012.06.038

Atienzar, P., Valencia, S., Corma, A., & García, H. (2007). Titanium-containing zeolites and microporous molecular sieves as photovoltaic solar cells. *ChemPhysChem, 8*, 1115–1119. doi:10.1002/cphc.200700019

Baerlocher, Ch., McCusker, L. B., & Olson, D. H. (2007). *Atlas of zeolite framework types, published on behalf of the structure commission of the international zeolite association* (6th ed.). Armsterdam: Elsevier.

Barton, T. J., Bull, L. M., Klemperer, W. G., Loy, D. A., McEnaney, B., Misono, M., … Yaghi, O. M. (1999). Tailored porous materials. *Chemistry of Materials, 11*, 2633–2656. doi:10.1021/cm9805929

Benkli, Y. E., Can, M. F., Turan, M., & Çelik, M. S. (2005). Modification of organo-zeolite surface for the removal of reactive azo dyes in fixed-bed reactors. *Water Research, 39*, 487–493. doi:10.1016/j.watres.2004.10.008

Carrero, A., Vicente, G., Rodríguez, R., Linares, M., & del Peso, G. L. (2011). Hierarchical zeolites as catalysts for biodiesel production from Nannochloropsis microalga oil. *Catalysis Today, 167*, 148–153. doi:10.1016/j.cattod.2010.11.058

Cejka, J., Corma, A., & Zones, S. (2010). *Zeolites and catalysis* (1st ed.). Morlenbach: Wiley-VCH Verlag. https://doi.org/10.1002/9783527630295

Corma, A., Fornes, V., Navarro, M. T., & Perezpariente, J. (1994). Acidity and stability of MCM-41 crystalline aluminosilicates. *Journal of Catalysis, 148*, 569–574. doi:10.1006/jcat.1994.1243

Corma, A., Rey, F., Valencia, S., Jordá, J. L., & Rius, J. A. (2003). A zeolite with interconnected 8-, 10- and 12-ring pores and its unique catalytic selectivity. *Nature Materials, 2*, 493–497. doi:10.1038/nmat921

Daramola, M. O., Aransiola, E. F., & Ojumu, T. V. (2012). Potential applications of zeolite membranes in reaction coupling separation processes. *Materials, 5*, 2101–2136. doi:10.3390/ma5112101

Eftekhari, S., Habibi-Yangjeh, A., & Sohrabnezhad, S. (2010). Application of AlMCM-41 for competitive adsorption of methylene blue and rhodamine B: Thermodynamic and kinetic studies. *Journal of Hazardous Materials, 178*, 349–355. doi:10.1016/j.jhazmat.2010.01.086

Esquivel, D., Cruz-Cabeza, A. J., Jiménez-Sanchidrián, C., & Romero-Salguero, F. J. (2013). Transition metal exchanged β zeolites: Characterization of the metal state and catalytic application in the methanol conversion to hydrocarbons. *Microporous Mesoporous Materials, 179*, 30–39. doi:10.1016/j.micromeso.2013.05.013

Fil, B. A., Ozmetin, C., & Korkmaz, M. (2012). Cationic dye (Methylene Blue) removal from aqueous solution by montmorillonite. *Bulletin of the Korean Chemical Society, 33*, 3184–3190. doi:10.5012/bkcs.2012.33.10.3184

Freundlich, H. M. F. (1906). Uber die adsorption in losungen. *Journal of Physical Chemistry, 57*, 385–470. doi:10.1515/zpch-1907-5723

Gougazeh, M., & Buhl, J.-Ch. (2014). Synthesis and characterization of zeolite a by hydrothermal transformation of Natural Jordanian Kaolin. *Journal of the Association of Arab Universities for Basic and Applied*

Science, 15, 35–42. doi:10.1016/j.jaubas.2013.03.007
Goursot, A., Coq, B., & Fajula, F. (2003). Corrigendum to toward a molecular description of heterogeneous catalysis: Transitional metal ions in zeolites. *Journal of Catalysis, 216*, 324–332. doi:10.1016/S0021-9517(02)00110-0
Hameed, B. H., Ahmad, A. A., & Aziz, N. (2007). Isotherms, kinetics and thermodynamics of acid dye adsorption on activated palm ash. *Chemical Engineering Journal, 133*, 195–203. doi:10.1016/j.cej.2007.01.032
Hameed, B. H., Ahmad, A. L., & Latiff, K. N. A. (2007). Adsorption of basic dye (methylene blue) onto activated carbon prepared from rattan sawdust. *Dyes and Pigments, 75*, 143–149. doi:10.1016/j.dyepig.2006.05.039
Hassani, M., Najafpour, G. D., Mohammadi, M., & Rabiee, M. (2014). Preparation, characterization and application of zeolite-based catalyst for production of biodiesel from waste cooking oil. *Journal of Scientific and Industrial Research, 73*, 129–133.
Jacobs, P. A., & Uytterhoeven, J. B. (1972). Assignment of the Hydroxyl Bands in the Infrared Spectra of Zeolites X and Y. *Heverlee: Centrum voor Oppervlaktescheikunde en Kolloïdale Schi-kunde. De croylaan*, 42, B-3030.
Kiricsi, I., Pál-Borbély, G., Nagy, J. B., & Karge, H. G., (Eds.). (1999). *Proceedings of the 1st International FEZA Conference, Surface Science and Catalysis* (pp. 1–824). Eger, Hungary: Elsevier Science.
Koohsaryan, E., & Anbia, M. (2016). Nanosized and hierarchical zeolites: A short review. *Chinese Journal of Catalysis, 37*, 447–467. doi:10.1016/S1872-2067(15)61038-5
Kwakye-Awuah, B., Von-Kiti, E., Nkrumah, I., & Williams, C. (2013). Effect of crystallization time on the hydrothermal synthesis of zeolites from kaolin and bauxite. *International Journal of Engineering Research and Technology, 2*, 1290–1300.
Langmuir, I. (1918). The adsorption of gases on plane surface of glass, mica and platinum. *Journal of the American Chemical Society, 40*, 1361–1403. doi:10.1021/ja02242a004
Lesničenoks, P., Grīnberga, L., & Kleperis, J. (2014). Gravimetric and Spectroscopic Studies of Reversible Hydrogen Sorption on Nanoporous Clinoptilolite. *Latvian Journal of Physics and Technical Sciences, N, 3*, doi:10.2478/lpts-2014-0017
Li, Y., Du, Q., Liu, T., Sun, J., Wang, Y., Wu, S., … Xia, L. (2013). Methylene blue adsorption on graphene oxide/calcium alginate composites. *Carbohydrate Polymers, 95*, 501–507. doi:10.1016/j.carbpol.2013.01.094
Marakatti, V. S., Halgeri, A. B., & Shanbhag, G. V. (2014). Metal ion-exchanged zeolites as solid acid catalysts for the green synthesis of nopol from Prins reaction. *Catalysis Science & Technology, 4*, 4065–4074. doi:10.1039/C4CY00596A
Mckay, G., & Ho, Y. S. (1999). Pseudo-second order model for sorption processes. *Process Biochemistry, 34*, 451–465. doi:10.1016/S0032-9592(98)00112-5
Nazila, E., Hossein, K., & Dariush, B. (2011). Synthesis of nano particles of LTA zeolite by means of microemulsion technique. *Iranian journal of Chemistry and Chemical Engineering, 30*, 1–8.
Opanasenko, M., Dhakshinamoorthy, A., Hwang, Y., Chang, J., Garcia, H., & Čejka, J. (2013). Superior performance of metalorganic frameworks over zeolites as solid acid catalysts in the prins reaction: Green synthesis of nopol. *Chemsuschem, 6*, 865–871. doi:10.1002/cssc.201300032
Pérez-Pariente, J., Díaz, I., Mohino, F., & Sastre, E. (2003). Selective synthesis of fatty monoglycerides by using functionalised mesoporous catalysts. *Applied Catalysis A: General, 254*, 173–188. doi:10.1016/S0926-860X(03)00481-2
Petrov, I., & Michalev, T. (2012). Synthesis of Zeolite A. *A Review, 51*, 1–30.
Qi, G., & Yang, R. T. (2005). Ultra-active Fe/ZSM-5 catalyst for selective catalytic reduction of nitric oxide with ammonia. *Applied Catalysis B: Environmental, 60*, 13–22. doi:10.1016/j.apcatb.2005.01.012
Qiu, H., Lv, L., Pan, B.-C., Zhang, Q.-J., Zhang, W.-M., & Zhang, Q.-X. (2009). Critical review in adsorption kinetic models. *Journal of Zhejiang University Science A, 10*, 716–724. https://doi.org/10.1631/jzus.A0820524
Rahmani, S., Azizi, S. N., & Asemi, N. (2016). Application of synthetic nanozeolite sodalite in drug delivery. *International Current Pharmaceutical Journal, 5*, 55–58. https://doi.org/10.3329/icpj.v5i6.27710
Sasidharan, M., & Kumar, R. (2004). Transesterification over various zeolites under liquid-phase conditions. *Journal of Molecular Catalysis A: Chemical, 210*, 93–98. doi:10.1016/j.molcata.2003.08.031
Seidel, A., & Bickford, M. (2013). *Kirk-Othmer Encyclopedia of Chemical Technology*. Hoboken: John Wiley & Sons Inc.
Sharma, P., Han, M. H., & Cho, C.-H. (2015). Synthesis of zeolite nanomolecular sieves of different Si/Al ratios. *Journal of Nanomaterials, 2015*, 9. doi:10.1155/2015/912575
Shirazi, L., Jamshidi, E., & Ghasemi, M. R. (2008). The effect of Si/Al ratio of ZSM-5 zeolite on its morphology, acidity and crystal size. *Crystal Research and Technology, 43*, 1300–1306. doi:10.1002/crat.200800149
Talesh, S. S. A., Fatemi, S., Hashemi, S. J., & Ghasemi, M. (2010). Effect of Si/Al ratio on CO2-CH4 Adsorption and Selectivity in Synthesized SAPO-34. *Separation Science and Technology, 45*, 1295–1301. doi:10.1080/01496391003684414
Tang, K., Wang, Y. G., Song, L. J., Duan, L. H., Zhang, X. T., & Sun, Z. L. (2006). Carbon nanotube templated growth of nano-crystalline ZSM-5 and NaY zeolites. *Materials Letters, 60*, 2158–2160. doi:10.1016/j.matlet.2005.12.088
Treacy, M. M. J., & Higgins, J. B. (2001). *Collection of simulated XRD powder patterns for zeolites*. Amsterdam: Elsevier on behalf of the Structure Commission of the International Zeolite Association.
Ugal, J. R., Hassan, K. H., & Ali, I. H. (2010). Preparation of type 4A zeolite from Iraqi kaolin: Characterization and properties measurements. *Journal of the Association of Arab Universities for Basic and Applied Sciences, 9*, 2–5. doi:10.1016/j.jaubas.2010.12.002
Vafajoo, L., Ghanaat, F., & Ghalebi, A. (2014). An investigation of a petrochemical wastewater treatment utilizing GAC: A study of adsorption kinetics. *APCBEE Procedia, 10*, 131–135. doi:10.1016/j.apcbee.2014.10.030
Vu, X. H., Armbruster, U., & Martin, A. (2016). Micro/mesoporous zeolitic composites: Recent developments in synthesis and catalytic applications. *Catalysts, 6*, 183. doi:10.3390/catal6120183
Wang, S., & Ariyanto, E. (2007). Competitive adsorption of malachite green and Pb ions on natural zeolite. *Journal of Colloid and Interface Science, 314*, 25–31. doi:10.1016/j.jcis.2007.05.032
Wang, S., & Peng, Y. (2010). Natural zeolites as effective adsorbents in water and wastewater treatment. *Chemical Engineering Journal, 156*, 11–24. doi:10.1016/j.cej.2009.10.029
Wang, S., & Zhu, Z. H. (2006). Characterisation and environmental application of an Australian natural zeolite for basic dye removal from aqueous solution. *Journal of Hazardous Materials, 136*, 946–952. doi:10.1016/j.jhazmat.2006.01.038
Yan, C., Wang, C., Yao, J., Zhang, L., & Liu, X. (2009). Adsorption of methylene blue on mesoporous carbons prepared using acid-and alkaline-treated zeolite X as the template. *Colloids and Surfaces A: Physicochemical and Engineering Aspects, 333*, 115–119. doi:10.1016/j.colsurfa.2008.09.028
Zaarour, M., Dong, B., Naydenova, I., Retoux, R., & Mintova, S. (2014). Progress in zeolite synthesis promotes advanced applications. *Microporous and Mesoporous Materials, 189*, 11–21. doi:10.1016/j.micromeso.2013.08.014
Zhang, H., Li, X., He, G., Zhan, J., & Liu, D. (2013). Preparation of magnetic composite hollow microsphere and its adsorption capacity for basic dyes. *Industrial & Engineering Chemistry Research, 52*, 16902–16910. doi:10.1021/ie402404z

Cogent Engineering **(ISSN: 2331-1916) is published by Cogent OA, part of Taylor & Francis Group.**